DØ Note 5727-CONF

A search for neutral higgs bosons at high $\tan\beta$ in the mode $\phi b \to \tau_\mu \tau_h b$ in RunIIb data

The DØ Collaboration
URL http://www-d0.fnal.gov
(Dated: August 2, 2008)

We report results from a search for neutral Higgs bosons decaying to tau pairs produced in association with a b-quark in the DØ Run IIb dataset of 1.2 fb^{-1}. The final states includes a muon, hadronically decaying tau, and jet identified as coming from a b-quark. We set cross section times branching ratio limits on production of such neutral Higgs bosons ϕ in the mass range from 90 GeV to 160 GeV. Exclusion limits are set at the 95% Confidence Level for several supersymmetric scenarios. A combination of these results with those from an earlier DØ analysis in this channel, and other related final states will follow.

Preliminary Results for Summer 2008 Conferences

I. INTRODUCTION

In models with supersymmetry (SUSY), the Higgs sector is expanded relative to the standard model (SM). In the minimal supersymmetric standard model (MSSM), which is a 2HDM type II model, two Higgs doublet fields are needed instead of one, and the resulting Higgs particle spectrum consists of two neutral scalars, a single neutral pseudoscalar and two charged scalars. The ratio of the vacuum expectation values of the two doublets is denoted $\tan\beta$, and the coupling to weak isospin $-1/2$ members of the fermion doublets becomes proportional to $\tan\beta$. For large values of $\tan\beta$ this gives significantly enhanced production cross sections to some processes, including $p\overline{p} \to \phi$ and $p\overline{p} \to \phi + b$ where ϕ is one of the neutral Higgs, $H/h/A$.

In the MSSM the dominant Higgs decay for a pseudoscalar Higgs mass (m_A) below ≈500 GeV is to a pair of b quarks, with τ pair decays occurring with a branching ratio of roughly 10%. However, the $p\overline{p} \to \phi b \to b\overline{b}b$ final state suffers from a large multijet background while the $b\tau\tau$ channel offers a much cleaner final state, giving the two channels similar sensitivities. In the mass range we consider, 90-160 GeV, two of the three the neutral higgs bosons will be nearly degenerate in mass and this overlap results in a factor of 2 gain in effective cross section.

In this analysis, results of a search for the reaction $p\overline{p} \to \phi b \to \tau\overline{\tau}b$ are presented. The final state includes a muon candidate, a hadronic tau candidate, and a jet tagged as a b-quark jet. This analysis builds on an earlier DØ result in the same final state[1].

II. DØ DETECTOR

The DØ detector has a central-tracking system, consisting of a silicon microstrip tracker (SMT) and a central fiber tracker (CFT), both located within a 2 T superconducting solenoidal magnet [2], with designs optimized for tracking and vertexing at pseudorapidities $|\eta| < 3$ and $|\eta| < 2.5$, respectively. During spring 2006, an additional layer for the silicon tracker was installed close to the beam pipe, improving charged particle momentum resolution and heavy flavor identification. Central and forward preshower detectors are positioned just outside of the superconducting coil. A liquid-argon and uranium calorimeter has a central section (CC) covering pseudorapidities $|\eta|$ up to ≈ 1.1, and two end calorimeters (EC) that extend coverage to $|\eta| \approx 4.2$, with all three housed in separate cryostats [3]. An outer muon system, at $|\eta| \approx 2$, consists of a layer of tracking detectors and scintillation trigger counters in front of 1.8 T toroids, followed by two similar layers after the toroids [4]. Luminosity is measured using plastic scintillator arrays placed in front of the EC cryostats. The trigger and data acquisition systems are designed to accommodate the high luminosities of Run II.

III. DATA SET AND MONTE CARLO SAMPLES

The data used in this analysis were recorded between June 2006 and July 2007. The recorded luminosity is approximately 1.4 fb^{-1}, and after applying data quality requirements 1.2 fb^{-1} remains. Data events are selected online using at least one of the possible nine high-p_T single muon triggers or one of twenty-four muon + hadronic tau triggers.

Backgrounds are estimated from a combination of simulated events and control data samples. Backgrounds arising from W, Z(+jets), $t\bar{t}$, WW and WZ production are computed using simulated events. The samples for $t\bar{t}$, WW and WZ processes are computed using the PYTHIA[5] event generator with the CTEQ6L1 parton distribution functions [6]. The vector boson (W, Z) + jets and (W, Z)+ heavy flavor ($c\bar{c}$, $b\bar{b}$)+ jets simulated samples were generated with ALPGEN[7], using PYTHIA for hadronization and showering. The normalization for the mulijet(QCD) backgrounds (in which at least one lepton arises from misidentification) are determined using data control samples.

The signal events were simulated using the SM $hb \to \tau_\mu \tau_h b + X$ process generated using PYTHIA for mass points from 90 to 160 GeV. The SM process is used to model our signal because the neutral Higgs bosons in SUSY are nearly degenerate in mass and behave in a very similar way to the SM Higgs.

All MC samples include overlay of minimum bias data with an instantaneous luminosity profile adjusted to match that of the data sample itself. This provides a realistic model of occupancy and other effects arising from increasing instantaneous luminosity. Simulated events are normalized using the theoretical cross section for the process, the acceptance times selection efficiency from simulation, and the luminosity of the data sample. The efficiencies from simulated events are corrected for differences in trigger and lepton identification efficiencies between data and simulation.

Neither PYTHIA nor ALPGEN reproduces the p_T spectrum of the Z boson in data. The simulated Z samples are therefore reweighted as functions of $p_T(Z)$ and jet multiplicity using weights derived from DØ $Z \to ee$ data. After the reweighting we normalize our backgrounds to their NNLO theoretical cross sections; $256^{+5.0}_{-11.0}$ pb for $Z \to \tau\tau$ [8]

as an example. We apply an additional factor of 1.9 to the $Wc\bar{c}, Zc\bar{c}, Wb\bar{b}$, and $Zb\bar{b}$ samples to take into account NNLO heavy-quark enhancement. This results in acceptable agreement between data and Monte Carlo.

IV. EVENT PRESELECTION

The final state includes one muon and one hadronic tau candidate. We require one muon in the event with p_T > 12 GeV, $|\eta| < 2.0$ and a central track match. In addition the muon must be isolated by requiring that the energy in the calorimeter within $0.1 < \Delta R < 0.4$ of the muon, or I_{cal}, must be less than 2.5 GeV, and that the sum of p_T of tracks within $0.0 < \Delta R < 0.5$ of the muon excluding the matched track, I_{trk}, must be less than 2.5 GeV. ΔR is defined as the distance in azimuth and rapidity, or $\Delta R = \sqrt{(\Delta(\eta)^2 + \Delta(\phi)^2}$. The track associated with the muon is constrained to originate from the beam spot if it does not have any SMT hits. There can be only one muon passing these requirements in the event. Events with more than one are discarded to reject $Z \to \mu\mu$ events and other backgrounds.

Hadronic tau decays are characterized by the presence of jets in the calorimeters and tracks in the tracking system. Identified hadronic taus are split into three types,

- Type 1: A calorimeter object having no EM subclusters and one charged track match. Analogous to $\tau \to \pi^{\pm}\nu$.
- Type 2: A calorimeter object having at least one EM subcluster with one charged track match. Analogous to $\tau \to \pi^{\pm}\pi^0\nu$.
- Type 3: A calorimeter object with or without EM subclusters and at least two charged tracks. Analogous to $\tau^{\pm} \to \pi^{\pm}\pi^{\pm}\pi^{\mp}\nu$.

We apply the following kinematic requirements on the hadronic tau E_T and associated track p_T:

- Type 1: E_T> 10 GeV, $p_T^{trk} > 7$ GeV
- Type 2: E_T> 10 GeV, $p_T^{trk} > 5$ GeV
- Type 3: E_T> 15 GeV, 1 track with p_T> 5 GeV, $\sum p_T^{trk} > 10$ GeV.

We additionally demand at least one SMT hit on one of the associated tracks and $E_T/p_T^{trk} > 0.65$ for types 1 and 2 only. We apply a Neural Network (NN_τ) to improve the purity of the selected taus. The neural network is trained separately for each tau type. The tau candidate NN_τ value must satisfy the following requirements

- Type 1: NN_τ> 0.9,
- Type 2: NN_τ> 0.9,
- Type 3: NN_τ> 0.95.

The tau must be separated from the isolated muon candidate and any other non-isolated muons in the event by requiring $\Delta R(\mu, \tau) > 0.5$. Finally we apply a correction to the Monte Carlo tau energy so that the calorimeter energy and track p_T ratio (E_T/p_T^{trk}) distribution matches the data in $Z \to \tau\tau$ events.

After muon and tau selection we require at least one good jet in the event, separated from the muon and tau by $\Delta R(\mu, jet) > 0.5$ and $\Delta R(\tau, jet) > 0.5$. The jet must have p_T> 15 GeV, $|\eta| < 2.5$ and $|\eta_{det}| < 2.5$ (where $|\eta_{det}|$ is the pseudorapidity measured from the detector's center), be confirmed in the Level 1 trigger system, and pass standard jet quality requirements. It must also be associated with the primary vertex in the event.

V. INSTRUMENTAL BACKGROUND ESTIMATION

We expect both heavy- and light- flavor multijet events (QCD) to pass the preselection. Simulations of these events poorly describe the data so the contribution is estimated from control data samples. To obtain a QCD-enriched control data sample, we apply the standard preselection but invert the muon isolation requirement; i.e. $2.5 < I_{cal} < 12.0$ and $2.5 < I_{trk} < 12.0$. Additionally we require that the tau has a NN output between 0.3 and 0.8 for all tau types. This reduces the contribution from $Z/\gamma^* \to \tau\tau$ and ensures that the QCD enriched sample will be orthogonal to the signal sample.

QCD (multijet) background events should have an equal number of mu-tau same-sign (SS) and opposite-sign (OS) events. To determine the number of QCD events in the signal sample before b-tagging we subtract the SS Standard Model MC backgrounds. The amount of QCD in the signal sample, N_{QCD}, is then

$$N_{QCD} = f_{QCD} N_{signal}(SS) \quad (1)$$

$$f_{QCD} = \frac{N_{rich}(OS)}{N_{rich}(SS)} \quad (2)$$

where $N_{rich}(OS)$ and $N_{rich}(SS)$ are the number of OS and SS events in the QCD enriched sample, respectively, and $N_{signal}(SS)$ is the yield in the control sample of events passing the signal selection requirements, except that the muon and tau are required to have the same sign after the same-sign Standard Model MC subtraction. This sample has negligible contamination from the Higgs signal and is dominated by QCD background.

Table I shows f_{QCD} for each of the three tau types.

τ Type	f_{QCD}
Type 1	1.031 ± 0.048
Type 2	1.090 ± 0.032
Type 3	1.046 ± 0.023
Average	1.057 ± 0.017
(χ^2/dof	1.6/2)

TABLE I: QCD scaling factors for each of the tau types, f_{QCD}, defined as $\frac{N_{rich}(OS)}{N_{rich}(SS)}$, and their statistical errors. We use the type-specific values in the analysis. The average and corresponding χ^2 are shown for information only.

To determine the QCD contribution after b-tagging, we take the average of two estimates as the final normalization. In the first method ("TRF method") we determine the probability for a jet to be b-tagged in the QCD-enriched sample described above, parametrize this probability as a function of jet p_T, and then apply this probability to the pre-tag QCD sample to determine the shape of the QCD events after tagging. In the second method (called the "Fake Rate Method") we prepare a sample with a b-tagged jet, a tau with $0.3 < NN_\tau < 0.9$, and a muon passing the usual kinematic cuts but ignoring the isolation values (the "no-iso" sample). We measure the muon isolation rate in events with $\not\!\!E_T < 20$ GeV, and then apply it to all events in the "no-iso" sample, and also apply a jet to tau fake rate measured in an independent $W \to \mu\nu+$ jets sample, giving the final number of QCD events in the second method. We take the QCD shape from the first method and normalize it to the average of the two methods, shown in Table II. We take half the difference between the two methods as the systematic on the QCD estimate.

τ Type	TRF Method	Fake Rate Method	Average
Type 1	4.94	1.73	3.34
Type 2	9.27	6.10	7.69
Type 3	7.17	4.22	5.69
Total	21.38	12.05	16.72

TABLE II: Total number of QCD events after final cuts including b-tagging for the different methods of estimation. We take the average of the TRF method and Fake Rate method as the overall normalization, and take the QCD shape from the TRF method.

VI. FINAL SELECTION

In our final signal sample we require the muon and tau to have opposite sign and the W mass variable,$M_W = \sqrt{\left(2\not\!\!E_T * (E^\mu)^2/p_T^\mu(1 - cos(\Delta\phi(\mu, \not\!\!E_T)))\right)}$, be less than 80, 80, and 60 GeV for events with tau types 1, 2 and 3, respectively. This is a useful cut to reduce W+jets background. The data and predicted background yields after the inclusive one-jet and b–tag selections are shown in Table III and for simulated signal in Table IV. Figure 1 shows the invariant mass of the $\mu, \tau, \not\!\!E_T$ system. We observe that the sample is dominated by $Z \to \tau\tau$ events before tagging.

The final selection requirement is the presence of at least one b-tagged jet tagged with a NN–based tagger. The typical b-jet tagging efficiency is 35% for jets in signal events and $Z+b\bar{b}$ production with a light flavor misidentification rate of 0.5%. Figure 2 shows the invariant mass of the $\mu, \tau, \not\!\!E_T$ system in the b–tagged sample. The background is now dominated by $t\bar{t}$ events.

	Tau Type 1	**Tau Type 2**	**Tau Type 3**	**All Tau Types**
μ, τ **Preselection**				
Data	565 ±24	2492 ±50	853 ±29	3910 ±63
Total pred.	542.9 ±16.8	2722.6 ±29.2	911.1 ±20.3	4203.5 ±49.5
$Z \to \tau\tau$	264.8 ±5.3	1910.8 ±20.5	536.0 ±7.6	2711.6 ±16.8
$Z \to \tau\tau$+hf	6.9 0.2	51.6 ±0.7	13.7 ±0.3	72.2 ±0.8
$Z \to \mu\mu$	27.9 ±1.9	181.3 ±5.0	20.7 ±1.5	229.8 ±4.5
$Z \to \mu\mu$+hf	0.50 ±0.06	4.5 ±0.2	0.50 ±0.05	5.5 ±0.2
$Z \to ee$	1.6 ±1.0	24.3 ±5.0	1.0 ±1.0	26.9 ±5.2
W+LP	20.9 ±2.3	111.4 ±5.4	50.7 ±3.4	183 ±6.8
W +HF	0.7 ±0.1	5.7 ±0.3	2.6 ±0.2	9.1 ±0.4
ttbar	1.0 ±0.2	23.3 ±0.9	1.9 ±0.3	26.2 ±1.0
Single Top	0.05 ±0.01	0.33 ±0.03	0.21 ±0.02	0.58 ±0.03
WW/WZ	2.8 ±0.2	44.6 ±0.9	2.8 ±0.2	50.1 ±0.9
QCD	217.4 ±15.5	389.1 ±23.2	282.0 ±18.4	888.5 ±32.2
$+ \geq 1$ **jet**				
Data	130 ±11	578 ±24	198 ±14	906 ±30
Total pred.	107.9 ±7.6	556.4 ±13.6	199.8 ±10.2	867.4 ±24.8
$Z \to \tau\tau$	44.9 ±1.6	318.5 ±6.0	90.0 ±3.2	453.3 ±5.0
$Z \to \tau\tau$+hf	3.0 ±0.2	23.9 ±0.4	6.2 ±0.2	33.1 ±0.5
$Z \to \mu\mu$	3.7 ±0.6	32.2 ±1.6	3.8 ±0.4	39.7 ±1.5
$Z \to \mu\mu$+hf	0.20 ±0.02	2.1 ±0.1	0.3 ±0.1	2.6 ±0.2
$Z \to ee$	0 ±0	3.6 ±2.0	0 ±0	3.6 ±2.0
W+LP	3.5 ±0.6	23.5 ±1.6	12.4 ±1.1	39.4 ±2.0
W +HF	0.3 ±0.1	3.1 ±0.2	1.4 ±0.1	4.9 ±0.3
ttbar	1.0 ±0.2	23.0 ±0.9	1.9 ±0.3	25.9 ±1.0
Single Top	0.04 ±0.1	0.3 ±0.02	0.2 ±0.02	0.55 ±0.03
WW/WZ	0.6 ±0.1	10.0 ±0.4	1.2 ±0.1	11.7 ±0.4
QCD	50.5 ±7.4	119.9 ±12.4	82.4 ±9.8	252.7 ±17.0
b**-tagging**				
Data	5.00 ±2.24	39.00 ±6.3	10.00 ±3.16	54±7.35
Total pred.	4.75 ±0.55	28.15 ±1.12	8.76 ±0.84	41.66 ±1.50
$Z \to \tau\tau$	0.22 ±0.01	1.56 ±0.02	0.44 ±0.01	2.22 ±0.03
$Z \to \tau\tau$+hf	0.46 ±0.03	3.72 ±0.09	0.95 ±0.04	5.13 ±0.10
$Z \to \mu\mu$	0.019±0.003	0.15 ±0.01	0.019 ±0.002	0.19 ±0.01
$Z \to \mu\mu$+hf	0.027 ±0.007	0.27 ±0.02	0.024 ±0.006	0.32 ±0.03
$Z \to ee$	0 ±0	0 ±0	0±0	0±0
W+LP	0.019 ±0.003	0.13 ±0.02	0.11 ±0.02	0.26 ±0.03
W +HF	0.05 ±0.01	0.34 ±0.03	0.17 ±0.02	0.56 ±0.04
ttbar	0.57 ±0.10	13.95 ±0.59	1.22 ±0.21	15.74 ±0.63
Single Top	0.019 ±0.004	0.12 ±0.01	0.09 ±0.01	0.23 ±0.01
WW/WZ	0.024 ±0.011	0.21 ±0.03	0.031 ±0.006	0.26 ±0.03
QCD	3.34 ±0.54	7.70 ±0.95	5.71 ±0.82	16.75 ±1.36

TABLE III: The predicted and observed event yields, with statistical errors, as a function of the selection requirements. We discuss the systematic errors in section VIII.

	$M_\phi = 100$ GeV		$M_\phi = 120$ GeV		$M_\phi = 140$ GeV		$M_\phi = 160$ GeV	
	Yield	Efficiency	Yield	Efficiency	Yield	Efficiency	Yield	Efficiency
Preselection	9.94	5.9%	6.51	5.5%	4.13	9.4%	2.49	7.6%
$+ \geq 1$ jet	4.95	49.8%	3.68	56.5%	2.26	54.7%	1.41	56.6%
b-tagging	1.85	37.4%	1.32	35.8%	0.79	39.8%	0.50	35.5%

TABLE IV: The predicted signals yields $\times 10^3$ as a function of the selection requirements. The yields before scaling by 10^3 use the cross sections predicted for $\tan\beta = 1$. The efficiency of the preselection is relative to the theoretical prediction.

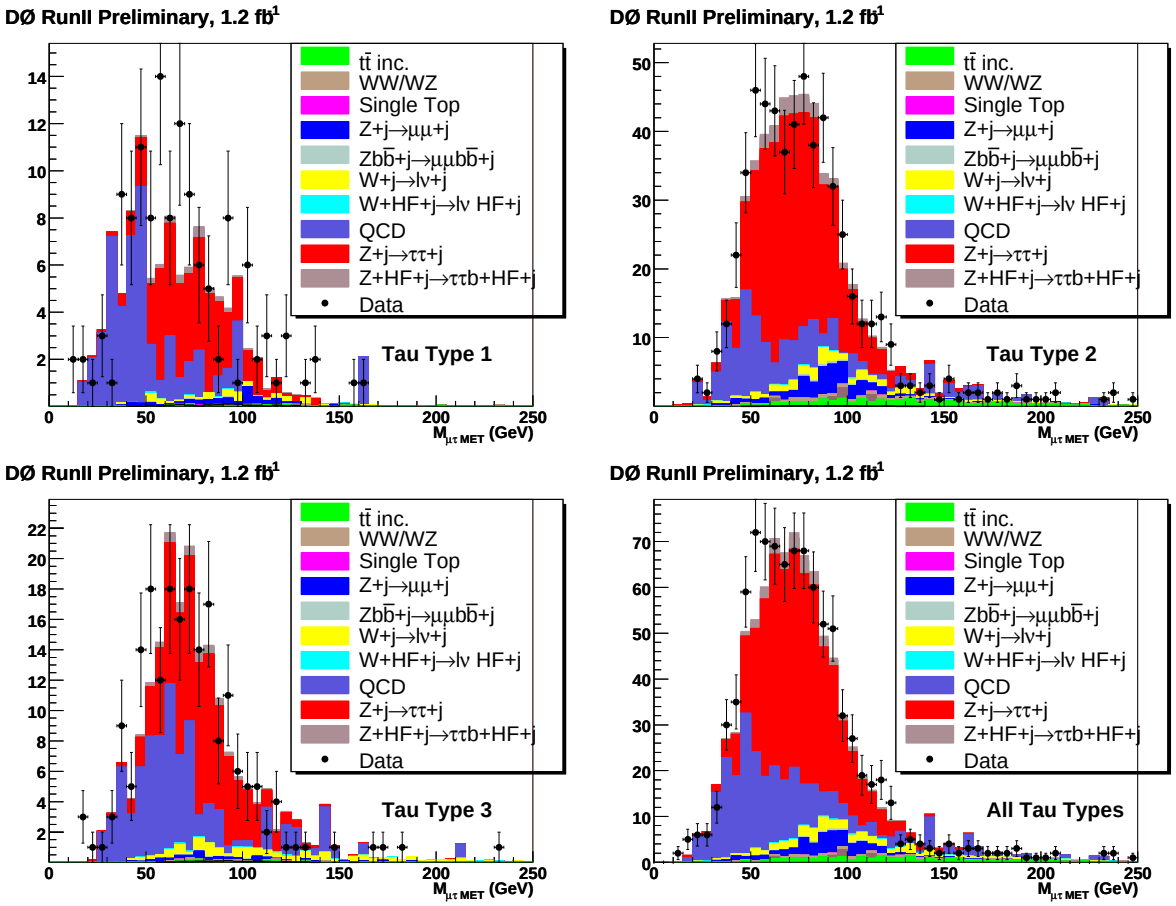

FIG. 1: Invariant mass of the $\mu, \tau, \not\!\!E_T$ system before b-tagging for: Type 1 taus (upper left), Type 2 (upper right), Type 3 (lower left), and all types (lower right.)

VII. MULTIVARIATE METHODS

After b-tagging events from $t\bar{t}$ and QCD multijet production dominate the background. It is difficult to find a single variable to cut in order to reduce the QCD or $t\bar{t}$ that does not also incur a substantial loss of signal, so we look to multivariate methods to reduce these two backgrounds. We use two separate techniques, one designed to reject $t\bar{t}$ events, and one to reject QCD. To reject $t\bar{t}$ background we apply a Kinematic Neural Network (KNN) originally developed in [1]. It uses the number of jets in the events, the sum of the tranverse momenta of the jets (HT), the energy from the four-momentum sum of the muon, tau, and jets, and the $\Delta\phi$ between the muon and tau candidate as input variables. A KNN cut of 0.3 typically offers $\approx 75\%$ rejection in $t\bar{t}$ with only a $\approx 4\%$ signal loss. To reject QCD we apply a simple unbinned log-likelihood ratio, trained separately for each signal mass point. We consider muon p_T, tau p_T, $\Delta R(\mu, \tau)$, $\mu - \tau$ invariant mass, and $(\mu, \tau, \not\!\!E_T)$ invariant mass, or visible mass, as input variables, and compute the likelihood of an event to be QCD-like or signal-like in all five variables, and then take the log of the

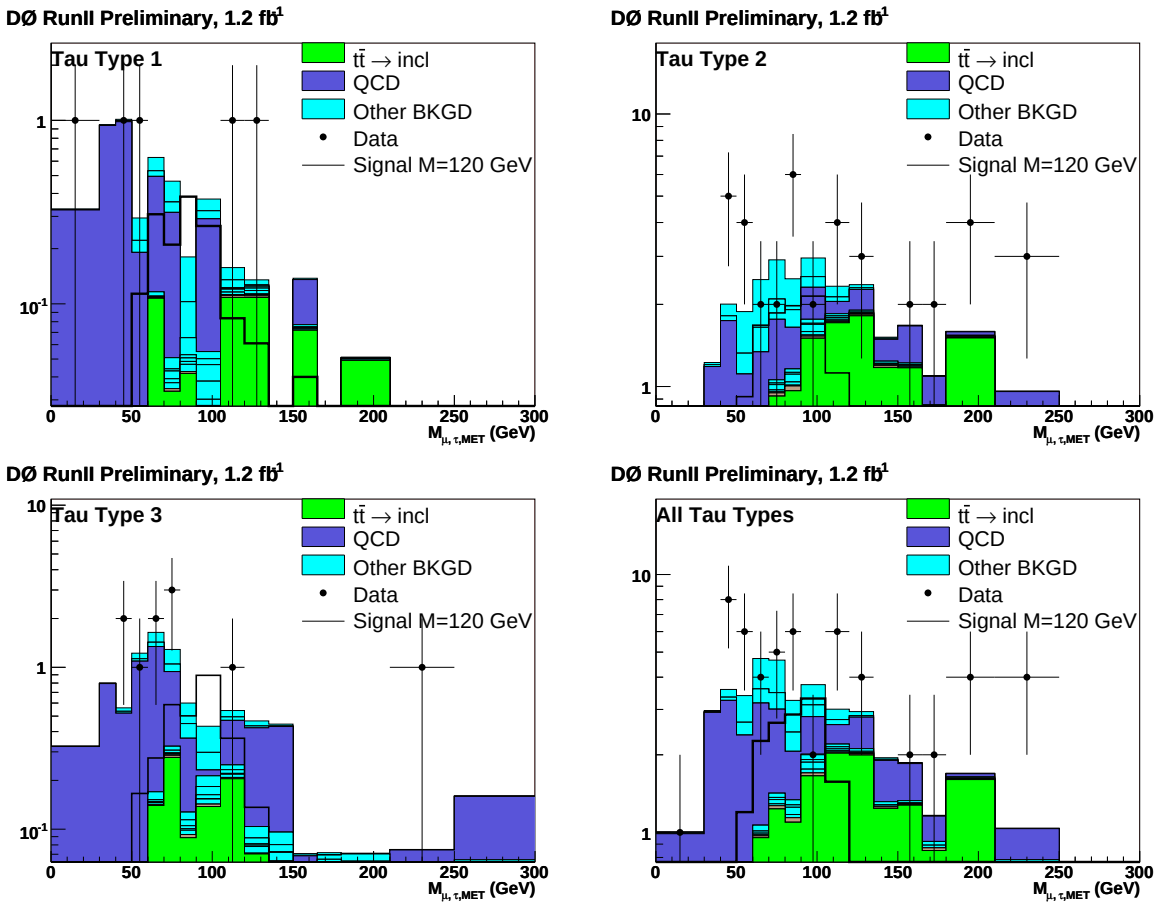

FIG. 2: Invariant mass of the $\mu, \tau, \not\!\!E_T$ system after b-tagging for: Type 1 taus (upper left), Type 2 (upper right), Type 3 (lower left), and all types (lower right.) The color scheme is identical in all four plots.

ratio of signal likelihood to QCD likelihood. Thus a high value is a signal-like event, while a low value is QCD-like. Figure 3 shows the KNN and QCD likelihood distributions for signal and background after b-tagging.

VIII. SYSTEMATIC UNCERTAINTIES

The sources of systematic uncertainty in this analysis include the Jet Energy Scale (JES), the jet identification efficiency and resolution, the b-tagging efficiency, the trigger efficiency, tau identification, luminosity, MC cross sections, and multjet background estimation. We calculate the uncertainties in the following ways:

- We determine the JES, Jet Reconstruction efficiency, trigger efficiency, and b-tagging efficiency uncertainties by shifting the relevant scale or event weight by $\pm 1\sigma$ and then calculating the new acceptances. Since these systematics are shape-driven, we denote them as "shape" in Table V and do not quote them as a percentage.
- The luminosity uncertainty is taken to be 6.1% [12].
- The τ ID/NN uncertainty is taken to be 8% in Type 1, 4% in Type 2, and 5% in Type 3 [10].
- The τ Energy Scale uncertainty is 3% for all types [11].
- We assign a 47% , 21% , and 26% systematic to the QCD calculation for tau types 1, 2, and 3, respectively, as described in Sec. V.
- We assign a shape-independent 10% uncertainty to the $W \to \ell\nu$+lp MC, 11% to the $t\bar{t}$ MC cross section, and 6% to tbe diboson MC cross section, and 12% to the Single Top MC cross section. We assign a +2%/-5%

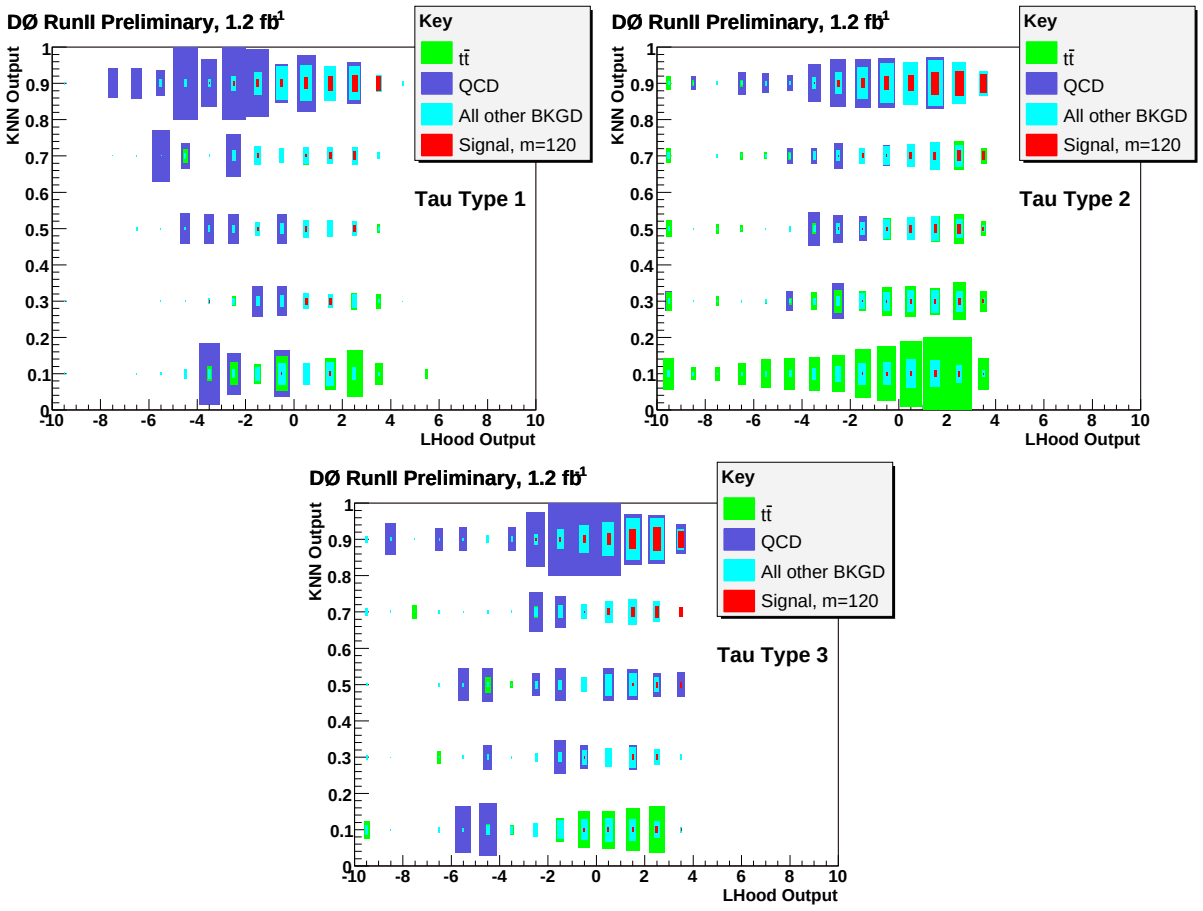

FIG. 3: KNN output vs. QCD likelihood output with 120 GeV signal for after b-tagging for: Type 1 taus (upper left), Type 2 (upper right), Type 3 (bottom.)

systematic uncertainty to the $Z \to \mu\mu$+lp MC and $Z \to \tau\tau$+lp MC cross sections, arising from the NNLO theory uncertainty. The $Z \to \tau\tau$+HF, $Z \to \mu\mu$+HF and $W \to \ell\nu$+HF MC have a 50% uncertainty, dominated by uncertainty on the K-factor of 1.9.

IX. LIMITS AND CONCLUSION

We cut on both the KNN and QCD likelihood in the 2D distributions of Fig. 3, using expected significance as the optimising variable, to determine the cross section limit. Table VI shows the KNN and QCD likelihood cuts for each mass point and tau type. We input the signal and background distributions of figure 3 after cuts into the standard DØ modified frequentist limit calculation program [13]. Once we have the cross section limits, shown in figure 4, we use FeynHiggs v2.6.2 [14] to interpret the limits in four Minimal Supersymmetric Standard Model (MSSM) scenarios: with no m_h-mixing and maximal m_h-mixing, and with $\mu = \pm 200$ GeV. Fig. 5 shows the expected and observed limits in the $\tan\beta$ vs. m_A plane. For m_A between 90 and 160 GeV we can exclude $\tan\beta$ above 100 in all four scenarios at all mass points.

[1] The DØ Collaboration, "Search for Neutral Higgs Bosons at high $\tan(\beta)$ in the $b(h/H/A) \to b\tau\tau$ Channel, `http://www-d0.fnal.gov/Run2Physics/WWW/results/prelim/HIGGS/H24`. Publication in preparation (p14, 340 pb^{-1})
[2] DØ Collaboration, V. Abazov *et al.*, Nucl. Inst. Meth. A 565, 463 (2006).
[3] DØ Collaboration, S. Abachi *et al.*, Nucl. Instrum. Methods Phys. Res. A **338**, 185 (1994).

Sample	Jet Energy Scale	Jet Reconstruction	b-tagging	Trigger	Luminosity	Tau NN	Tau ES	QCD	MC Cross section
Signal	shape	shape	shape	shape	6.1%	3-8%	3%	–	–
$Z \to \tau\tau$+lp	shape	shape	shape	shape	6.1%	3-8%	3%	–	+2/-5%
$Z \to \tau\tau$+HF	shape	shape	shape	shape	6.1%	3-8%	3%	–	50%
$Z \to \mu\mu$+lp	shape	shape	shape	shape	6.1%	3-8%	3%	–	+2/-5%
$Z \to \mu\mu$+HF	shape	shape	shape	shape	6.1%	3-8%	3%	–	50%
W+lp	shape	shape	shape	shape	6.1%	3-8%	3%	–	10%
W+HF+lp	shape	shape	shape	shape	6.1%	3-8%	3%	–	50%
$t\bar{t}$	shape	shape	shape	shape	6.1%	3-8%	3%	–	11%
WW/WZ	shape	shape	shape	shape	6.1%	3-8%	3%	–	6%
Single Top	shape	shape	shape	shape	6.1%	3-8%	3%	–	12%
QCD Type 1	–	–	–	–	–	–	–	47%	–
QCD Type 2	–	–	–	–	–	–	–	21%	–
QCD Type 3	–	–	–	–	–	–	–	26%	–

TABLE V: Systematic uncertainties applied to each signal and background sample. For shape dependent systematics, denoted as "shape" in the table, we vary the effect by $\pm 1\sigma$, then use the resulting distributions as inputs to the limit setting program and fit with a profile likelihood. Those systematics expressed as a perecentage are taken as flat systematics and are input into the limit setting program accordingly. The dashes ("–") mean that the systematic in that column is not applied to the MC sample in that row.

	Type 1		Type 2		Type 3	
Higgs Mass	KNN Cut	LHood cut	KNN Cut	LHood cut	KNN Cut	LHood cut
90	0.2	-1	0.3	-1	0.2	-1
100	0.3	-2	0.3	-1	0.2	0
110	0.3	-2	0.4	-2	0.2	-1
120	0.2	-2	0.35	-2	0.2	-1
130	0.2	-2	0.35	-2	0.2	-1
140	0.3	-2	0.35	-2	0.2	0
150	0.3	-2	0.35	-2	0.2	-1
160	0.2	-2	0.3	-3	0.2	-1

TABLE VI: Values of KNN and QCD likelihood cut for each mass point and tau type.

[4] V. Abazov *et al.*, "The Muon System of the Run II DØ Detector", physics/0503151.
[5] T. Sjöstrand *et al.*, Comput. Phys. Commun. **135**, 238 (2001).
[6] H.L. Lai *et al.*, Phys. Rev. D **55**, 1280 (1997).
[7] M.L. Mangano, M. Moretti, F. Piccinini, R. Pittau, A. Polosa, JHEP **307** 1 (2003).
[8] R. Hamberg, W.L. van Neerven and T. Matsuura, Nucl. Phys. B **359**, 343 (1991) and errata in **644**, 403. A.D. Martin, R.G. Roberts, W.J. Stirling, R.S. Thorne, Phys. Lett. B **604** 61-68 (2004).
[9] DØ Collaboration, V. M. Abazov et al., Phys. Rev. D **71**, 072004 (2005).
[10] M. Owen, W.-C. Yang, S. Söldner-Rembold, M. Titov, FERMILAB-PUB-08/132-E, submitted to PRL (2008).
[11] M. Owen, A. Patwa, S. Söldner-Rembold, W.C. Yang, DØ Note 5708 (2008).
[12] T. Andeen et al, FERMILAB-TM-2365-E (2006).
[13] W. Fisher, FERMILAB-TM-2386-E.
[14] M. Frank, T. Hahn, S. Heinemeyer, W. Hollik, H. Rzehak, G. Weiglein, JHEP **702** 047 (2007).
G. Degrassi, S. Heinemeyer, W. Hollik, P. Slavich, G. Weiglein, Eur.Phys.J. **C28** 133-143 (2003).
S. Heinemeyer, W. Hollik, G. Weiglein, Eur.Phys.J. C9 343-366 (1999).
S. Heinemeyer, W. Hollik, G. Weiglein, Comput.Phys.Commun. **124** 76-89 (2000).

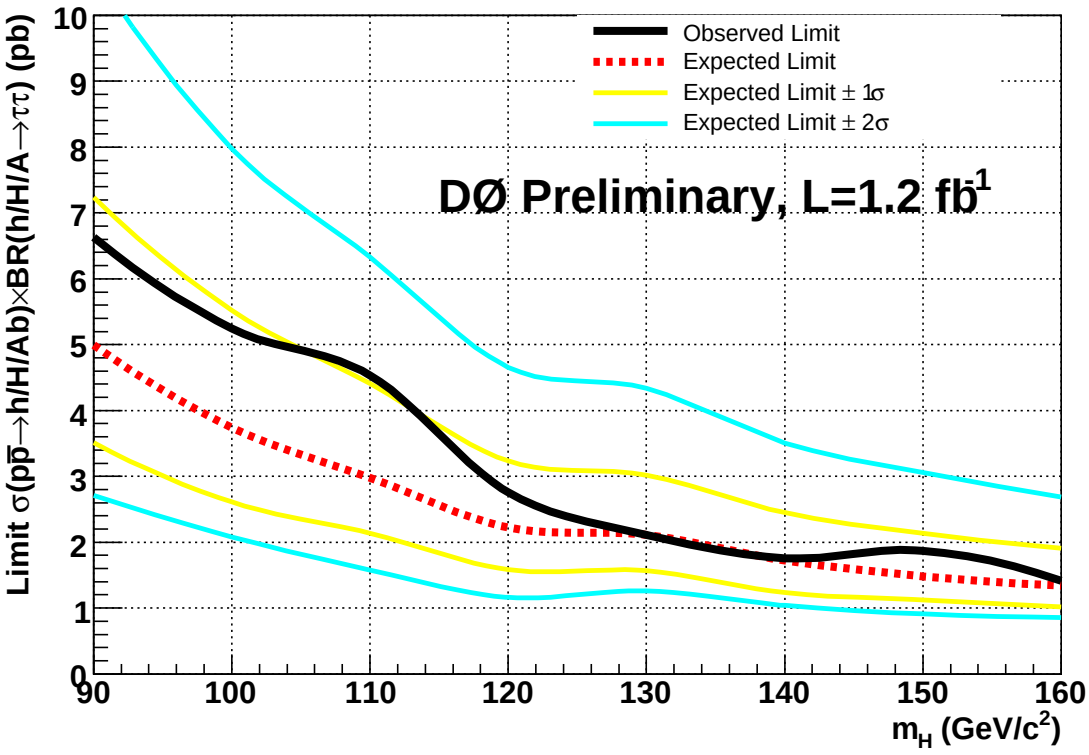

FIG. 4: Expected and observed cross section × BR limits vs. Higgs mass.

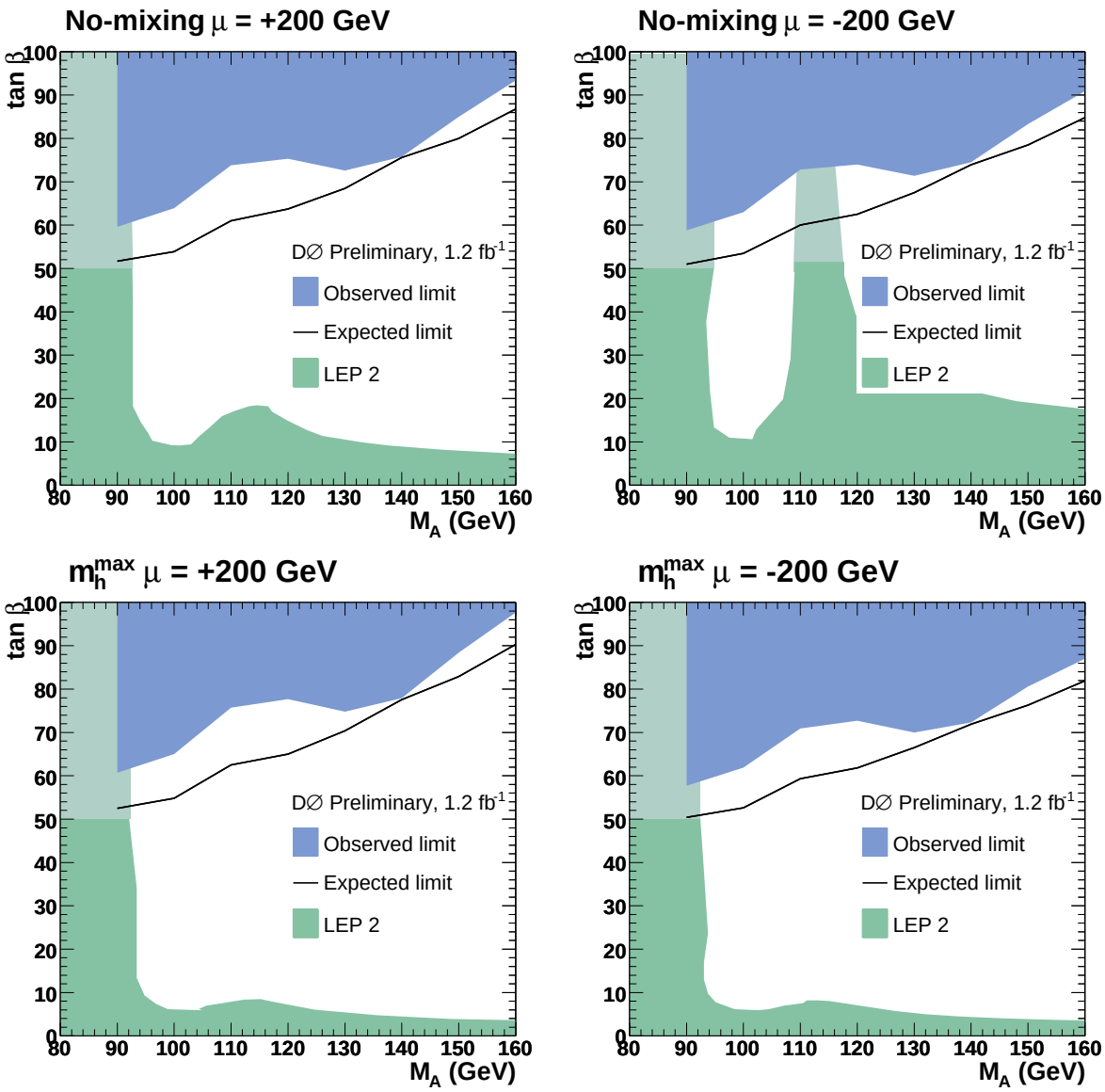

FIG. 5: Limits on $\tan\beta$ vs. M_A for the no-mixing, $\mu > 0$ case (upper left); no-mixing, $\mu < 0$ case (upper right); maximal-mixing, $\mu > 0$ case (lower left); maximal-mixing, $\mu < 0$ case (lower right).